Physica B 457 (2015) 156–159

Contents lists available at ScienceDirect

Physica B

journal homepage: www.elsevier.com/locate/physb

Scanning thermoelectric microscopy of local thermoelectric behaviors in $(Bi,Sb)_2Te_3$ films

Kunyu Zhao [a], Huarong Zeng [a,*], Kunqi Xu [a,b], Huizhu Yu [a,b], Guorong Li [a], Junqiang Song [c], Xun Shi [c], Lidong Chen [c]

[a] Key Laboratory of Inorganic Functional Materials and Devices, Shanghai Institute of Ceramics, Chinese Academy of Sciences, Shanghai 200050, China
[b] University of Chinese Academy of Sciences, Beijing 00039, China
[c] State Key laboratory of High Performance Ceramics and Superfine Microstructures, Shanghai Institute of Ceramics, Chinese Academy of Sciences, Shanghai 200050, China

ARTICLE INFO

Article history:
Received 15 August 2014
Received in revised form
30 September 2014
Accepted 7 October 2014
Available online 16 October 2014

Keywords:
Seebeck coefficient
Thermal conductivity
$(Bi,Sb)_2Te_3$ (BST) thermoelectric thin films
Scanning thermoelectric microscopy (STeM)

ABSTRACT

In this paper we develop scanning thermoelectric microscopy (STeM) on the basis of commercial atomic force microscope. The nanoscale thermoelectric behaviors of $(Bi,Sb)_2Te_3$ (BST) thin films were studied. 3ω-technique was used for thermal conductivity imaging and quantitative thermal characterization. By acquiring the unique Seebeck information from 2ω frequency component, nanoscale thermoelectric images were firstly obtained, exhibiting remarkably inhomogeneous distribution of local Seebeck coefficient in the thin films. Positive thermoelectric response is revealed by the modulation of temperature difference between thermal tip and sample, corresponding to p-type conduction within BST sample.

1. Introduction

Thermoelectric films have received increasing interests due to their application potential on electronic devices in the micro-heating and cooling areas in the past decade. Lots of investigations have been performed to explore the corresponding thermoelectric properties and the way to enhance the thermoelectric properties of the thermoelectric films prepared by different methods [1–5]. In thermoelectric materials, the thermoelectric figure of merit ZT which is the only criterion to estimate thermoelectric energy conversion efficiency, is defined as $ZT=\alpha^2\sigma T/\kappa$, here α, σ, T and κ are the Seebeck coefficient, electrical conductivity, thermal conductivity, and absolute temperature, respectively. In recent years, tremendous efforts have been devoted to unveiling the approach of qualitative and quantitative characterization on thermoelectric materials, including α, σ, κ with the resolution of micrometer even sub-micrometer scale [6–12]. Since nanostructured thin films have emerged as a promising candidate owing to their unique advantages of enhancing ZT via decreasing local thermal conductivity, studying the thermoelectric effects and properties of low dimensions and local structures is critical for the performance assessment and device exploitation for thermoelectric materials. Nevertheless, the investigations of nanoscale thermoelectric characteristics are still insufficient, and the non-destructive high resolution imaging of distribution with respect to local Seebeck coefficient has been rarely reported.

Scanning probe techniques provides a non-destructive, ultra-high resolution tool to visualize nanoscale structures and to evaluate local physical properties. In the past few decades, superfine thermal probes with thermocouples at the end of metallic wire have been adopted to profile local temperature and thermal properties [13]. Development of scanning probe microscope (SPM) and scanning tunnel microscope (STM) facilitate nanoscale quantitative measurement of the Seebeck voltage of p–n junction in semiconductor materials and nanostructures in thermoelectric bulk samples generated by nano-thermometers[14]. Very recently, investigations have been performed to quantitatively determine thermal conductivity and Seebeck coefficient simultaneously by a microprobe technique in which an alternative current joule-heated V-shaped microwire has been used as heater, thermometer and voltage electrode [12]. However, for further application it is still necessary to understand local thermoelectric effect of nanostructured thermoelectric materials. Especially, high resolution imaging of local thermoelectric effect has never been reported. In this work, scanning thermoelectric microscope (STeM) based on

* Corresponding author. Fax: +86 21 52413122.
E-mail address: Huarongzeng@mail.sic.ac.cn (H. Zeng).

http://dx.doi.org/10.1016/j.physb.2014.10.009
0921-4526/

commercial SPM was developed and the locally thermoelectric properties and effects of $(Bi,Sb)_2Te_3$ (BST) films were studied.

2. Experiment

$(Bi,Sb)_2Te_3$ thin films were fabricated using a magnetron co-sputtering system with base pressure lower than 1.0×10^{-4} Pa. High-purity (99.99%) bismuth, antimony, and tellurium targets with diameter of 3 in. were used as source materials. Bismuth and antimony targets were each connected to a direct-current (DC) power supply, and the tellurium target was connected to a radiofrequency (RF) power supplier. All films were deposited at room temperature on silicon (001) substrates with 300 nm thermally grown oxide layer and 300 nm nitride layer grown by plasma-enhanced chemical vapor deposition (PECVD). The distance between the targets and the substrate was kept at 65 mm, and substrates were rotated at 22 rpm for uniform film deposition. The DC power was set to 6 W for Bi and 12 W for Sb, and the RF power was set to 62 W for Te. The working pressure was set at 0.3 Pa, flowing 50 sccm Ar as sputtering gas. The thermal treatment of the samples was performed in a vacuum annealing furnace with base pressure lower than 1.0 Pa. The samples were annealed with a heating rate of 10 K/min under Ar atmosphere at pressure of about 1.0×10^{-4} Pa and maintained for 4 h at 150 °C. Then the sample was cooled down without forced cooling.

STeM was set up on a conventional scanning probe microscope (SPA 400, SPI3800N, Seiko Inc. Japan), as shown in Fig. 1. In STeM, a resistive thermal element is adopted, consisting of a bent filament (5 μm diameter) of platinum/10% rhodium surrounded by a thick silver cladding of 75 μm diameter. The contact area between sample and probe has been determined to be 30 nm [15]. The resistive probe is heated up periodically by a large current from an external functional generator (33120A, Agilent Inc.). In this case, a temperature modulation occurs within the tip and the probe induces thermal waves into the sample. Heat flows from the tip to the sample and the probe acts as a heater. As the heated tip makes a nanoscale contact with the sample, a localized temperature gradient is created in the sample near the contact point. The frequency multiplier will multiply the modulation frequency from the signal generator to the reference frequency of 2ω and/or 3ω and acts as the reference to the lock-in amplifier (Model 7280 DSP, signal recovery instrumentation). Additionally, the direct electric signal from the film is recorded by digital multi-meter (Tektronix DMM 4050), reflecting local thermoelectric effect quantitatively.

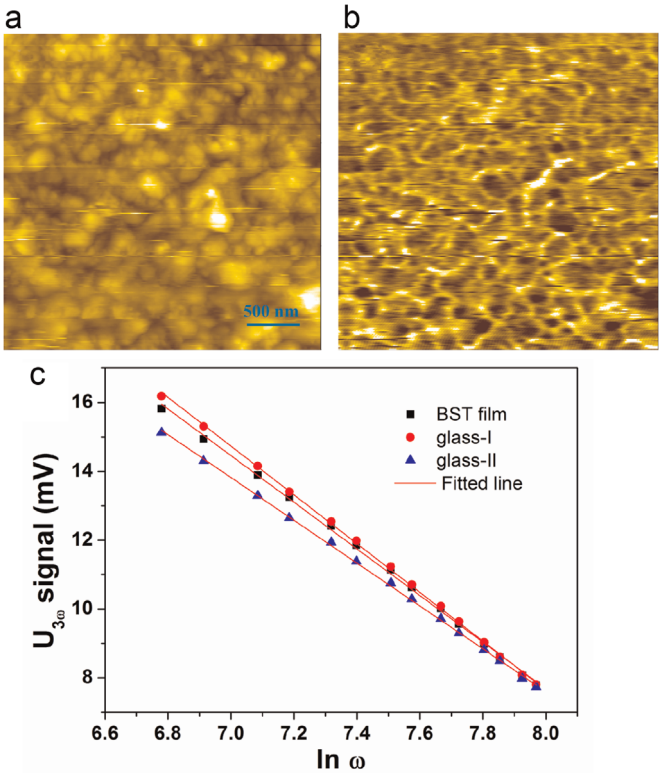

Fig. 2. Topography image (a) and its in-situ thermal image (b) of BST sample. (c) The 3ω-output voltage signal of the Wheatstone bridge as a function of thermal excitation frequency for BST film (■), glass-I (●), glass-II (▲).

3. Results and discussion

Firstly, the qualitative and quantitative investigation of local thermal conductivity were performed on the basis of 3ω-technique [16]. Fig. 2a and b shows the topography image and corresponding thermal image of BST sample on 2 μm × 2 μm scanning area. The polycrystalline film is relatively smooth with root mean square roughness (rms) values of about 9 nm. Interestingly, most BST grains exhibit darker contrast in Fig. 2b, indicating lower thermal conductivity, whereas grain boundaries have relatively higher thermal conductivity.

Using the 3ω-technique, we hereby measure local $U_{3\omega}$ signals at different excitation modulation frequencies (f). Local $U_{3\omega}$ signals of BST thin films in the frequency range from 140 Hz to 460 Hz are

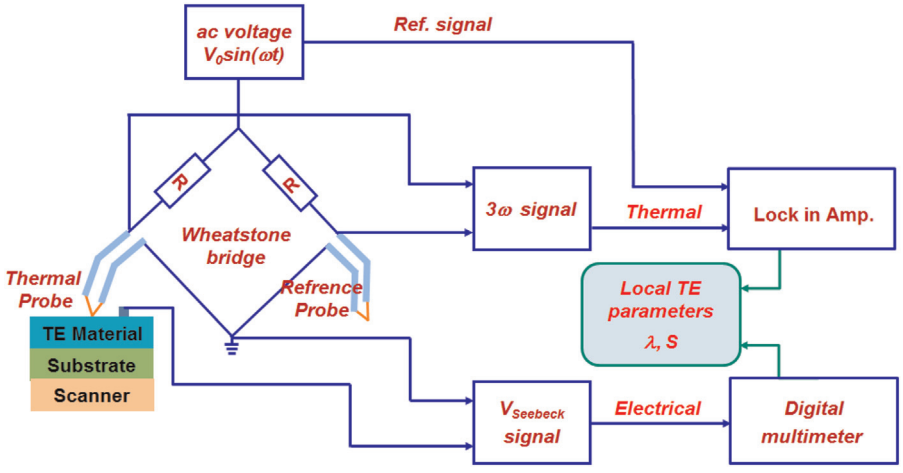

Fig. 1. Schematic set-up of the scanning thermoelectric microscopy.

given in Fig. 2c, in which the lateral axis is the logarithm of angular frequency ($\omega=2\pi f$). According to the principle of 3ω-technique, ω-pulsation will excite a 3ω-signal component of the output voltage of the Wheatstone bridge, which can be expressed by$U3\omega 1$ where λ (W/m K) is the thermal conductivity of the sample, R (Ω) the electrical resistance, T (°K) the temperature, l the thermal probe length, dR/dT is the corresponding differential coefficient. It can be found that there is a linear proportionality between the local 3ω-signal and ln (ω). Such linear proportional relation can be observed from the fitted lines for BST thin films in Fig. 2c.

The near-field thermal model proposed by Altes et al. [16] was adopted in the present work to calculate the local λ values. For the specimen with low thermal conductivity ($\lambda \leq 10$ W/m K), the general term can be expressed as$U3\omega 1-U3\omega 2\ln(\omega 1)-\ln(\omega 2)=k1\lambda$ where the coefficients k_1 and k_2 can be obtained by two reference samples. Two glass specimens (glass-I and glass-II) were used in this work for reference samples. Glass-I was an $MgO–Al_2O_3–SiO_2–TiO_2$ system glass with thermal conductivity of 2 W/m K, while Glass-II was a normal glass provided by Samsung Corning Co. Ltd., with thermal conductivity of 0.8 W/m K. Both reference samples were polished to optical grade with a thickness of 2 mm. Within the experimental frequency range, the local 3ω-signals of the reference samples exhibit the same variation trend with the BST films, as shown in Fig. 2c. Based on Eq. (2) and with a combination of the related data of two reference samples, the local thermal conductivity for BST thin films was calculated to be 1.66 W/m K, which is in good accordance with the macroscopic value (1.7 W/m K) [17].

In STeM, the 3ω method uses a narrow metal as a heater and thermal probe, which passes through a current with an angle frequency of ω. The resulting periodic heat generation of the narrow meter due to the Joule effect which is proportional to the square of the current, can be expressed by$P(t)=1/2R(t)I02[1-\cos(2\omega t)]$. Hence the heating power on the sample is varied with the angle frequency 2ω. The temperature fluctuation of the sample can be determined by the resistance change of the narrow metal, which is proportional to the heating power with the angle frequency 2ω. It should be noticed that the temperature oscillation of the films includes the heat generated by either Joule effect or Peltier effect (contains the component of ω), herein the Joule effect is dominant over the Peltier effect by about two orders of magnitude [10,18]. Thus the propagation of the 2ω temperature fluctuation can give rise to the Seebeck effect, namely an in-plane 2ω voltage fluctuation signal will be generated. Consequently, the analysis of 2ω component of the Seebeck voltage signal would facilitate to acquire the isolated material specific thermoelectric properties.

Fig. 3a and b shows the topography image and corresponding thermoelectric image of the BST sample on 2 μm × 2 μm scanning area. The thermoelectric image in Fig. 3b was obtained with reference modulation frequency at 200 Hz as described previously. In spite of the influence from local morphology, the contrast of thermoelectric image was expected to reflect the discrimination of local Seebeck coefficient. It is reasonable to deduce that brighter contrast area in thermoelectric image represents the local structure with higher Seebeck coefficient since the larger Seebeck voltage output caused by the carrier transport under temperature potential in imaging procedure. The in-situ line scan signals of Fig. 3a and b are given in Fig. 3c. The distribution of thermoelectric signal shows significantly independent variation comparing with the topographic fluctuation, revealing local inhomogeneity of Seebeck coefficient in BST films, which is tightly related to the local carrier concentration distribution of such A_2B_3 compounds [19].

For the further investigation of thermoelectric properties on nanoscale, local thermoelectric behavior of BST thin films is

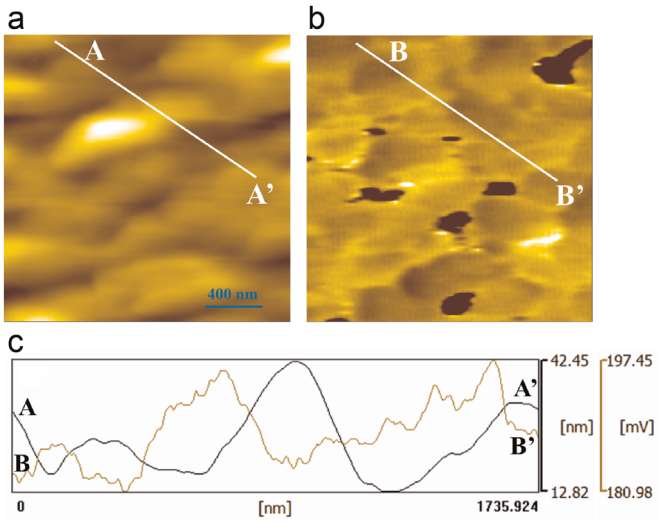

Fig. 3. Topography image (a) and its in-situ thermoelectric image (b) of BST sample (c) line scan image of topographic (a) and thermoelectric (b) signal.

investigated. Fig. 4a shows the relationship between the Seebeck signal $U_{Seebeck}$ and the effective input excitation voltage, a nonlinear dependence is revealed. The probe resistance which was obtained by balancing the Wheatstone bridge, also increased with the increasing input power, corresponding to the positive temperature coefficient of the Pt/Rd probe (insert of Fig. 4a). The value of the Seebeck voltage rises more rapidly at higher input voltage, which might be caused by the nonlinear probe temperature variation versus the input voltage, as shown in Fig. 4b. The modulation of excitation voltage can give rise to a temperature difference of approximately 20 °C at the thermal probe. Fig. 4c shows the Seebeck voltages and its variation with ΔT_{probe}, indicating a positive value of Seebeck coefficient, which is expected for BST films with a p-type conduction. In the A_2B_3 compounds, the conduction mechanism (p or n type) is determined by the type of the dominant carrier. In $(Bi_xSb_{1-x})_2Te_3$, both Sb and Bi have the same trend of forming Sb_{Te} and Bi_{Te} antisites, which would serve as acceptors and cause p-type conduction behavior [20]. It is noted that quantitatively thermoelectric characterization is a dynamic process with continuous thermoelectric interaction between the thermal tip and the sample surface. The effective thermal exchange radius r_{th} would essentially determine the precision of the results. Several investigations have been devoted to estimating the effective thermal exchange radius of the Wollaston thermal tip by different theoretical models, the r_{th} at the value ranging from 200 nm to 2 μm were reported, and is generally thought to be around 1 μm, meaning that the thermoelectric behavior exhibited in Fig. 2 reflected the local characteristic within the small area of effective thermoelectric interaction range [12,21]. Although the local thermoelectric response of BST thin films exhibiting remarkable stability in our study (Fig. 4d), more efforts have been paid on the improvement of scanning probe thermoelectric techniques in the further investigation in order to get a deep insight in to the local properties of such kind of thermoelectric thin films.

4. Conclusion

In summary, nanoscale thermoelectric behavior of $(Bi,Sb)_2Te_3$ thin films was investigated by scanning thermoelectric microscopy developed based on commercial atomic force microscope. Local thermal conductivities are characterized quantitatively and qualitatively via 3ω-method. Nanoscale thermoelectric images are

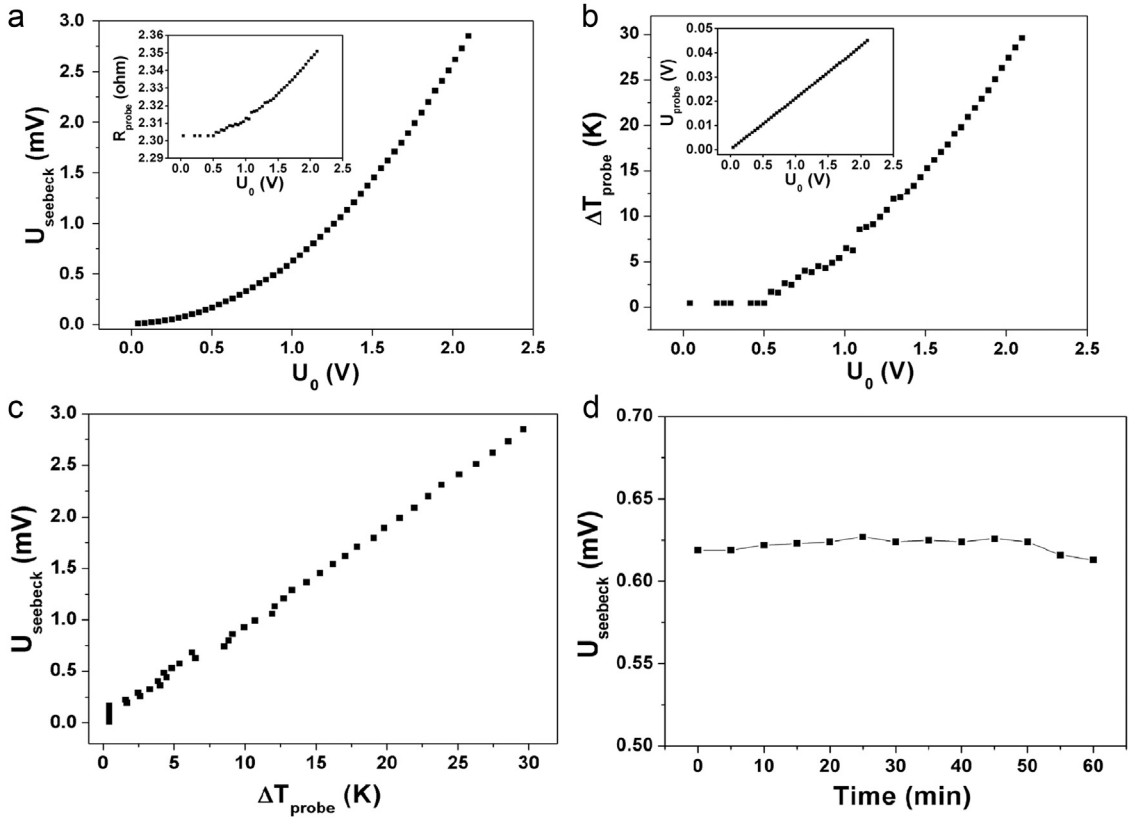

Fig. 4. (a) Seebeck voltage of BST plotted as a function of exciting voltage, insert of (a) is the variation of probe resistance versus the exciting voltage. (b) Temperature rise of thermal probe plotted as a function of exciting voltage, insert of (b) is the increase of probe voltage versus the exciting voltage. (c) Seebeck voltage of the sample plotted as a function of the probe temperature rise, insert of (c) shows the time stability of the probe-sample system.

firstly obtained, reflecting inhomogeneous distribution of local Seebeck coefficient in the BST material. Positive thermoelectric response corresponding to p-type conduction within BST films is observed by the modulation of temperature difference between thermal tip and sample. The results show that STeM is a promising tool for qualitative and quantitative thermal characterization in thermoelectric materials on sub-micrometer or even nanometer scale.

Acknowledgement

This work is supported by the National Basic Research Program of China under Grant nos. 2012CB933004 and 2015CB654605, the National Natural Science Foundation of China under Grant nos. 51121064 and 51402328, the Nanotechnology Project of Shanghai Science and Technology Committee under Grant no. 11nm0502800, International Science & Technology Cooperation Program of China (Nos. 2013DFR50800 and 2013DFG51570), and the Bureau of International Co-operation Chinese Academy of Sciences.

References

[1] R. Venkatasubramanian, E. Siivola, T. Colpitts, B. O'Quinn, Nature 413 (2001) 597–602.
[2] R. Geethu, R. Jacob, T. Shripathi, G.S. Okram, V. Ganesan, S. Tripathi, A. Fatima, P.V. Sreenivasan, K.S. Urmila, B. Pradeep, R.R. Philip, Appl. Surf. Sci. 258 (2012) 6257–6260.
[3] G. Joshi, H. Lee, Y.C. Lan, X.W. Wang, G.H. Zhu, D.Z. Wang, R.W. Gould, D.C. Cuff, M.Y. Tang, M.S. Dresselhaus, G. Chen, Z.F. Ren, Nano Lett. 8 (2008) 4670–4674.
[4] C.N. Liao, K.M. Liou, H.S. Chu, Appl. Phys. Lett. 93 (2008) 042103.
[5] Z.G. Zeng, P.H. Yang, Z.Y. Hu, Appl. Surf. Sci. 268 (2013) 472–476.
[6] M.K. Jacobsen, W. Liu, B. Li, Rev. Sci. Instrum. 83 (2012) 093903.
[7] S.J. Kim, J.H. We, G.S. Kim, B.J. Cho, J. Appl. Phys. 112 (2013) 104511.
[8] N. Chen, F. Gascoin, G.J. Snyder, E. Muller, G. Karpinski, C. Stiewe, Appl. Phys. Lett. 87 (2005) 171903.
[9] T.T. Miao, W.G. Ma, X. Zhang, J. Vac. Sci. Technol. B 30 (2012) 051804.
[10] T.T. Miao, W.G. Ma, X. Zhang, Z. Li, Rev. Sci. Instrum. 82 (2011) 024901.
[11] B. Yang, J.L. Liu, K.L. Wang, G. Chen, Appl. Phys. Lett. 80 (2002) 1758–1760.
[12] Y.L. Zhang, C.L. Hapenciuc, E.E. Castillo, T. Borca-Tasciuc, R.J. Mehta, C. Karthik, G. Ramanath, Appl. Phys. Lett. 96 (2010) 062107.
[13] U.F. Wischnath, J. Welker, M. Munzel, A. Kittel, Rev. Sci. Instrum. 79 (2008) 073708.
[14] H.K. Lyeo, A.A. Khajetoorians, L. Shi, K.P. Pipe, R.J. Ram, A. Shakouri, C.K. Shih, Science 303 (2004) 816–818.
[15] L.J. Balk, M. Maywald, R.J. Pylkki, in: Proceedings of the 9th Conference on Microscopy of Semiconducting Materials, Institute of Physics Conference Series. Vol. 146, 1995, pp. 655–658.
[16] A. Altes, R. Heiderhoff, L.J. Balk, J. Phys. D: Appl. Phys. 37 (2004) 952–963.
[17] H. Scherrer, S. Scherrer, Thermoelectric Properties of Bismuth Antimony Telluride Solid Solutions, in: D.M. Rowe (Ed.), Thermoelectrics Handbook: Macro to Nano, CRC Press, Boca Raton, 2005 (27-16).
[18] H.H. Roh, J.S. Lee, D.L. Kim, J. Park, K. Kim, O. Kwon, S.H. Park, Y.K. Choi, A. Majumdar, J. Vac. Sci. Technol. B 24 (2006) 2398–2404.
[19] J.Q. Song, X.H. Chen, Y.S. Tang, Q. Yao, L.D. Chen, J. Electron. Mater. 41 (2012) 3068–3072.
[20] Z.L. Sun, S.C. Liufu, X.H. Chen, L.D. Chen, ACS Appl. Mater. Interfaces 3 (2011) 1390–1393.
[21] E. Puyoo, S. Grauby, J.M. Rampnoux, E. Rouviere, S. Dilhaire, Rev. Sci. Instrum. 81 (2010) 073701.